Isolated Metal Atom Geometries as a Strategy for Selective Heterogeneous Hydrogenations

Georgios Kyriakou, *et al.*

Science **335**, 1209 (2012);
DOI: 10.1126/science.1215864

Isolated Metal Atom Geometries as a Strategy for Selective Heterogeneous Hydrogenations

Georgios Kyriakou,[1] Matthew B. Boucher,[2] April D. Jewell,[1] Emily A. Lewis,[1] Timothy J. Lawton,[1] Ashleigh E. Baber,[1] Heather L. Tierney,[1] Maria Flytzani-Stephanopoulos,[2] E. Charles H. Sykes[1]*

Facile dissociation of reactants and weak binding of intermediates are key requirements for efficient and selective catalysis. However, these two variables are intimately linked in a way that does not generally allow the optimization of both properties simultaneously. By using desorption measurements in combination with high-resolution scanning tunneling microscopy, we show that individual, isolated Pd atoms in a Cu surface substantially lower the energy barrier to both hydrogen uptake on and subsequent desorption from the Cu metal surface. This facile hydrogen dissociation at Pd atom sites and weak binding to Cu allow for very selective hydrogenation of styrene and acetylene as compared with pure Cu or Pd metal alone.

Typical heterogeneous catalysts for hydrogenation reactions often contain noble metals and alloys based on platinum, palladium, rhodium, and ruthenium. Although these metals are active at modest temperature and pressure for a variety of heterogeneous hydrogenations, including alkenes and alkynes, they are not always selective toward the desired product and are expensive. Given that molecular hydrogen (H_2) dissociation is often the rate-limiting step, one strategy is to engineer the minimal catalytic ensemble that will activate H_2 but not the other reactants. Along these lines, several studies have shown that individual atoms of Pt, Pd, or Au in charged or ionic states supported on oxides can efficiently catalyze a number of important reactions (*1*–*4*). Our recent work provides evidence that, in the Pt catalyzed water-gas shift reaction, it is not the metal nanoparticle as such but an ionic species stabilized on the surface of the oxide support that functions as the active site for catalytic turnover (*3*).

In a different but related thrust, we are interested in how the reactivity of a catalytically active metal is altered when it is atomically dispersed in the surface layer of a more inert host metal. Such an approach, if successful, would offer a means to both temper the reactivity of a very active element and to design catalysts with very small amounts of the precious metal. Besenbacher *et al*. showed that the opposite strategy can be effective in reducing the reactivity of a metal by adding small amounts of Au to a Ni surface to prevent coking of the Ni and improve steam-reforming performance (*5*). In a series of low-temperature scanning tunneling microscopy (LT-STM) and density functional theory (DFT) studies, we investigated the formation of a class of bimetallic alloy systems, which we term single-atom alloys (SAAs), and their interaction with H_2 (*6*–*8*). Two key characteristics of SAAs are (i) the more active of the two components (in our case Pd) is present in the surface of the host metal at very low concentrations [~0.01 monolayer (ML)] and (ii) atoms of the more active component (Pd) are thermodynamically more stable when surrounded by the host metal such that no dimers or trimers are present at low coverage. Theory predicts in a simple homogeneous surface slab that Pd:Cu ratios up to 1:2 yield individual, isolated Pd atoms that are more stable when surrounded by Cu as compared with Pd dimers or trimers (*6*).

This effect is depicted in the STM image in Fig. 1 for a 0.01 ML Pd in Cu (111) [Pd/Cu(111)] alloy surface (*9*). Detailed investigation of the alloying process reveals that, depending on the substrate temperature upon Pd deposition, alloying occurs mainly in either the topmost layer (~350 K) or in the subsurface layers at a higher sample temperature (~500 K) (*6*–*8*, *10*). The evaporated Pd adatoms adsorb on the substrate and diffuse over the terraces in a random walk fashion until they are trapped at the nearest ascending step edge where place exchange and alloying into the copper surface layer takes place. DFT calculations by Sholl and co-workers (*7*) reveal that, despite the relatively low barrier of Pd to traverse step edges, it binds very strongly to ascending step edges, and we find experimentally that it remains there during subsequent reaction.

The Pd/Cu SAA surface displays a rather uncommon energetic landscape for the dissociation and chemisorption of hydrogen. Unlike Pd, the pristine Cu(111) surface is inert toward the dissociation of unactivated H_2 in ultrahigh vacuum (UHV) because of the dissociation barrier on the order of 0.4 eV (*11*). Critically, we find that a small quantity of Pd atoms in the Cu surface makes the SAA active toward the uptake of H_2, which can dissociate on the Pd monoatomic entities and then spill over onto the bare Cu(111) terraces. Chopra *et al*. recently reported a related effect involving Ti_2Al_2 complexes in a Ti-doped Al(111) surface that efficiently activated H_2 (*12*). Also, Wittstock *et al*. suggested that, in the case of the oxidative coupling of methanol, the activity of nanoporous Au, prepared by dealloying of AuAg alloys, may be rationalized either by a local change of the d-band structure or by dissociation of oxygen on Ag followed by spillover onto the Au (*13*). LT-STM (5 K) enabled us to directly visualize individual hydrogen adatoms (H_a) on the Cu(111) surface that spilled over from Pd atom sites in a 0.01 ML Pd/Cu(111) surface after exposure to ~10 Langmuirs (L, 10^{-6} torr·s) of H_2 at 80 K (Fig. 1C). Hydrogen atoms appear as depressions in the STM images because of the lower electron tunneling probability through the H-metal complex as compared with the bare metal at energies near the Fermi level (typically <0.1 eV) (*14*, *15*).

Temperature-programmed desorption (TPD) measurements of H_2 desorption from Pd/Cu were acquired after exposing two different Pd coverages (Fig. 2A, 0.01 ML Pd, and Fig. 2B, 0.1 ML Pd) to H_2 at 85 K. In both cases, the alloys were prepared by depositing Pd on Cu(111) at a sample temperature of 380 K for appropriate time intervals in order to generate surfaces with different densities of Pd atoms substituted into the surface layer. Desorption of H_2 from the 0.01 ML Pd/Cu(111) alloy surface (Fig. 2A) occurred in a

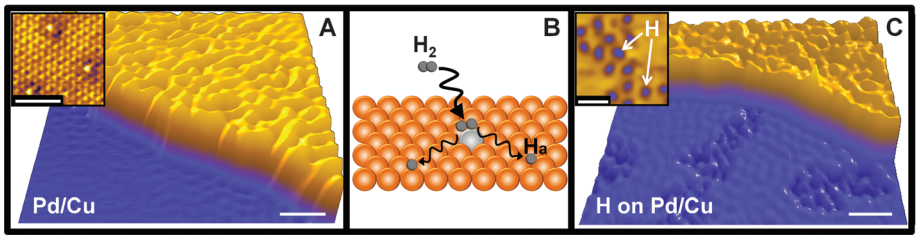

Fig. 1. STM images showing atomically dispersed Pd atoms in a Cu(111) surface and hydrogen atoms that have dissociated and spilled over onto the Cu surface. (**A**) Pd alloys into the Cu(111) surface preferentially above the step edges as evidenced by the rumpled appearance of the upper terrace (scale bar indicates 5 nm). (Inset) Atomic resolution of the Pd/Cu alloy on the upper terrace showing individual, isolated Pd atoms in the surface layer appearing as protrusions (scale bar, 2 nm). (**B**) Schematic showing H_2 dissociation and spillover at individual, isolated Pd atom sites in the Cu surface layer. (**C**) Islands of H atoms imaged after hydrogen uptake appear as depressed regions on the clean Cu(111) lower terrace (scale bar, 5 nm). (Inset) High-resolution image of individual hydrogen atoms on Cu(111) (scale bar, 2 nm). Images recorded at 5 K.

[1]Department of Chemistry, Tufts University, 62 Talbot Avenue, Medford, MA 02155, USA. [2]Department of Chemical and Biological Engineering, Tufts University, 4 Colby Street, Medford, MA 02144, USA.

*To whom correspondence should be addressed. E-mail: charles.sykes@tufts.edu

single state that initially shifted to lower temperatures upon increasing the H_a coverage, as expected for a second-order desorption process. A 200-L H_2 exposure yielded a surface H_a coverage of 0.2 ML. The peak maximum (210 K) was much lower than that expected for H_2 desorption from Cu(111) (310 K) (*16*) or Pd(111) (320 K) (*17*). This effect demonstrates that individual, isolated Pd atoms both assist adsorption and spillover of H_a onto Cu(111) by acting as the dissociation site for H_2 and, as would be expected from microscopic reversibility, serve as low-barrier exit routes for H_2 during the desorption process. In comparison, desorption of H_2 from Cu(111) occurs at ~310 K because of a large recombination barrier and from Pd(111) at ~320 K because of strong binding. Theoretical modeling has indicated that at higher Pd:Cu ratios two-atom Pd ensembles are best for activating H_2 (*18*), but our data in the very low coverage regime reveal that Pd monomers in the Cu surface are sufficient to induce the low-temperature hydrogen activation and desorption observed here.

Increasing the surface concentration of Pd to 0.1 ML yielded an even lower H_2 desorption maximum (175 K) compared with that of the 0.01 ML Pd/Cu(111) surface for the same nominal H_2 exposure; the amount of H_2 desorbing from the surface (~0.4 ML) increased by a factor of 2 for the same 200-L exposure. The increase of the H_a surface coverage coupled with the even lower desorption temperature suggests that increasing the number of Pd monoatomic entities in the surface effectively increases the number of entrance and exit routes of hydrogen on and off the Cu(111) surface. Surface strain also serves to lower the H_2 desorption temperature, because the addition of larger Pd atoms (diameter d_{Pd} = 0.275 nm) to a smaller Cu(111) lattice (d_{Cu} = 0.256 nm) imparts compressive strain in the surface. This weakens the binding of H to the Pd atoms from which they desorb, resulting in a lower desorption temperature (*19*). Further increases of the Pd coverage to 1 ML (Fig. 2C) resulted in broad desorption features that saturated after small H_2 doses with an H_a coverage ~0.7 ML. These desorption profiles are consistent with a rather heterogeneous surface of energetically different adsorption sites ranging from Pd monoatomic entities to 2-ML-high Pd islands, which shifted the desorption feature to higher temperatures, as expected for desorption of H_2 from Pd(111) or high Pd content Pd/Cu alloys (*17*, *18*).

The potential energy diagram shown in Fig. 3 illustrates the vastly different energetics of the interaction of hydrogen with Pd(111), Cu(111), and Pd/Cu SAAs. Energies and activation barriers are taken from (*6*, *20*). The Pd(111) and Cu(111) surfaces display a difference in the dissociative adsorption of hydrogen. Although H_2 dissociation on Pd(111) is not activated (activation energy $E_a \approx 0$ eV), on Cu(111) it is hampered by a rather large activation barrier of 0.4 eV. Conversely, the binding energy of H_a on Cu(111) is about 0.2 eV, which is much weaker than that on Pd(111) (0.6 eV) (*6*, *20*). The weak binding of H_a on, and activated desorption of H_2 from Cu versus the strong binding of H_a on, and nonactivated desorption of H_2 from Pd lead to almost identical H_2 desorption temperatures from both surfaces (310 to 320 K). The situation, however, is drastically different on Pd/Cu SAA surfaces.

Our TPD data revealed that single Pd atoms in the Cu(111) surface lowered the activation barrier to H_2 dissociation and bound H_a weakly enough to allow it to spill over onto the Cu surface. The net effect is a surface that can easily activate H_2 dissociation (as evidenced by efficient uptake at 85 K) but also bind it weakly. A similar type of behavior has been theoretically predicted for a related class of surface alloys termed near-surface alloys (NSAs) (*20*, *21*). NSAs involve a single layer of one metal either supported on or sandwiched between layers of a different host metal. Such NSAs have been shown to form even when bulk alloys are not thermodynamically stable. It is predicted that, in addition to binding reactants more weakly than the corresponding pure metals, NSAs can also dissociate reactants more readily. The important catalytic properties of NSAs have been demonstrated with both model single-crystal alloy surfaces and nanoparticle catalysts (*22*–*24*). For example, a single Ni layer on Pt(111) exhibits increased activity in the reforming of oxygenates as compared with Pt(111), a subsurface Ni ML, or a thick Ni layer on Pt(111) (*23*). RuPt core-shell nanoparticles also display enhanced reactivity in the preferential oxidation of CO in the presence of H_2 feed as compared with traditional PtRu nanoalloys, monometallic mixtures of nanoparticles, and pure Pt particles (*24*). By contrast, our SAAs are not layer-on-layer like the NSAs but use an extremely low surface concentration of the active metal in the surface layer, thus allowing the host surface to preserve its original properties. In the present case, the Cu(111) host surface, which is in overwhelming excess (99:1), binds H_a weakly.

Inspired by this vastly different energetic landscape for hydrogen adsorption and desorption, we investigated the capacity of Pd/Cu SAAs to perform low-temperature, selective catalytic hydrogenations by using two probe molecules: styrene and acetylene. Styrene serves as a model alkene in UHV studies (*25*) because it can bond strongly to metals through π interactions. The heterogeneously catalyzed hydrogenation of trace acetylene to ethene is of major industrial importance, and the adsorption of acetylene has also been extensively studied on both Cu(111) and Pd(111) by various techniques (*26*, *27*). Figure 4A shows representative data acquired from a 0.01 ML Pd/Cu(111) SAA after adsorbing 0.2 ML of H_a followed by 0.5 ML of styrene. The sole hydrogenation product of the reaction of styrene with H_a was ethylbenzene, which desorbed at 260 K with a 13% conversion and >95% selectivity based on the detection limit of our mass spectrometer. Unreacted styrene also desorbed during the

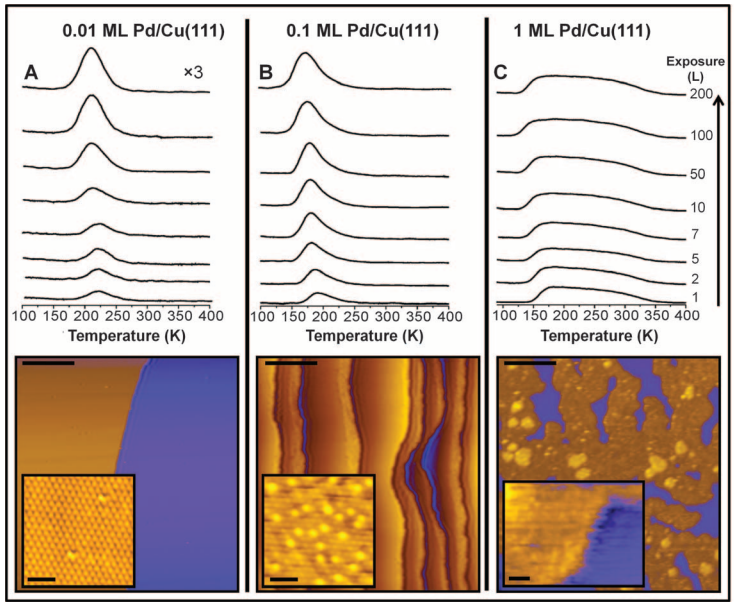

Fig. 2. TPD of H_2 as a function of Pd coverage and corresponding STM images of Pd/Cu(111) surface alloys. (**A**) H_2 uptake on 0.01 ML Pd/Cu(111); STM image of 0.01 ML Pd/Cu(111) showing that the low Pd coverage leaves the Cu(111) surface mostly unaffected. (Inset) High-resolution image of a region above a step edge where individual Pd surface atoms reside. (**B**) H_2 uptake on 0.1 ML Pd/Cu(111); STM image of 0.1 ML Pd/Cu(111). The step edges appear scalloped because of the formation of a denser substitutional alloy on their upper terrace. (Inset) High-resolution image in the vicinity of the step edge where the Pd/Cu(111) surface alloy consisting predominantly of Pd monomers can be seen. (**C**) H_2 uptake on 1 ML Pd/Cu(111); STM image of 1 ML Pd/Cu(111) showing the onset of 2 ML high Pd island formation before completion of the first layer. (Inset) Image of the Pd island and Cu(111) interface. The scale bars in all full-size STM images are 20 nm, and the scale bars of the insets are 3 nm.

temperature-programmed reaction (TPR) sweep, with all desorption features being essentially identical to what is expected for styrene adsorption on clean Cu(111) (figs. S1 and S3). This reveals that the very small amount of Pd in the Cu(111) surface (1:99) does not alter the adsorption properties of the molecule. The absence of any high-temperature H_2 desorption features indicates that there is essentially no decomposition of styrene on the 0.01 ML Pd/Cu(111) surface. In other words, the single Pd atoms have converted the otherwise entirely inactive Cu(111) surface into an effective and very selective hydrogenation catalyst by providing both a low-energy entrance route for H_a and many Cu sites where it is weakly bound.

The Pd/Cu SAA also catalyzed the hydrogenation of acetylene to ethene with high selectivity. Earlier work by Lambert and co-workers (*27*) has shown that desorption of acetylene from the clean Cu(111) surface produces ethene (8% conversion) through decomposition and self-hydrogenation of acetylene at ~330 K, as well as small quantities of coupling products (mainly benzene desorbing at ~320 K). Figure 4B and fig. S4 show representative TPR spectra for the hydrogenation of acetylene on a 0.01 ML Pd/Cu(111) SAA after adsorbing 0.2 ML of H_a and 0.5 ML of acetylene. Hydrogenation of acetylene proceeded via two distinct pathways. The high-temperature (330 K) pathway is similar to the TPR of acetylene from Cu(111) in the absence of any preadsorbed Pd or H_a (fig. S1), and we assigned this pathway to the decomposition and self-hydrogenation of acetylene at high temperatures on Cu(111) (*27*). The conversion of acetylene in the high-temperature pathway is estimated to be 14% (ethene, 4%; surface carbon, 8%; and benzene, 2%). The low-temperature ethene formation pathway, in which acetylene reacts with preadsorbed H_a on Cu(111), corresponds to 3% conversion of the initially adsorbed acetylene with >95% selectivity based on the detection limit of our mass spectrometer.

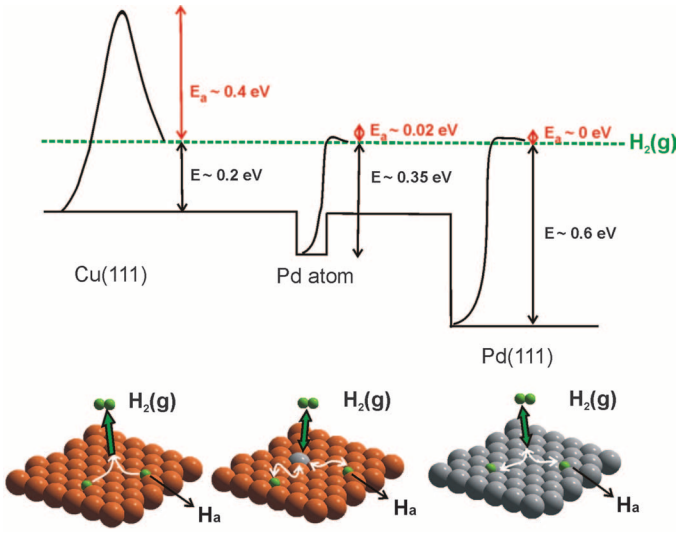

Fig. 3. Potential energy diagram depicting the mode of action of a Pd SAA surface compared with those of pure Cu(111) and Pd(111). Dissociative adsorption of H_2 on Cu(111) (orange) is a highly activated process. On Pd(111) (gray), H_2 dissociation is practically barrierless, but the adsorbed atoms are bound strongly. In the case of an isolated Pd atom, the dissociation barrier is low, hydrogen is weakly bound, and it can spill over onto the Cu(111) surface.

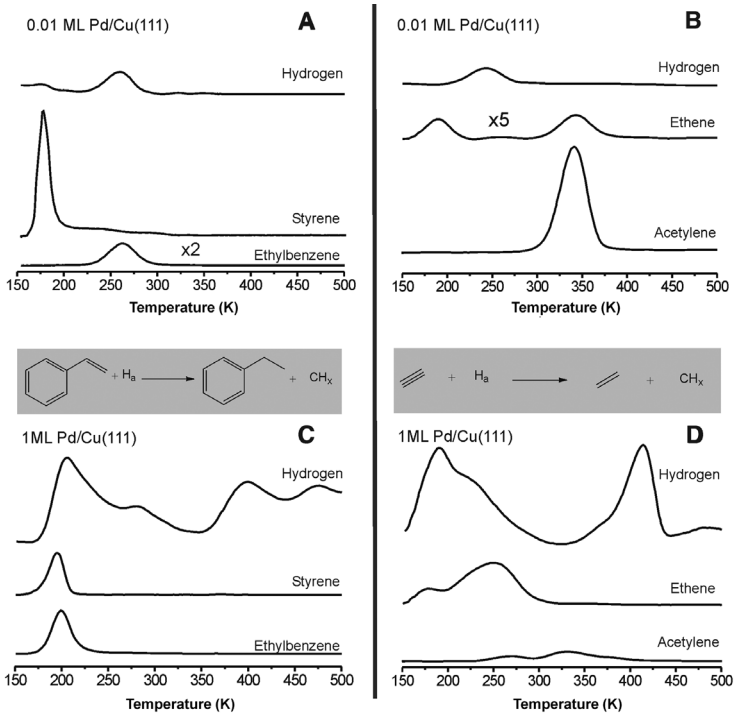

Fig. 4. Representative TPR data showing the increase in selectivity obtained by atomically dispersing Pd atoms in Cu versus the extensive decomposition of the reactants on a 1-ML Pd layer. (**A**) Styrene hydrogenation on 0.01-ML Pd/Cu(111) alloy. (**B**) Acetylene hydrogenation on 0.01-ML Pd/Cu(111) alloy surface. (**C**) Styrene hydrogenation on 1-ML Pd/Cu(111) alloy. (**D**) Acetylene hydrogenation on 1-ML Pd/Cu(111). In all cases, near-saturation H_a was deposited at 85 K followed by 0.5 ML of the hydrocarbon at 150 K.

In marked contrast to the selective hydrogenation chemistry on SAAs, the hydrogenation of styrene and acetylene on 1 ML Pd/Cu(111) (Fig. 4, C and D) was accompanied by an extensive decomposition of both molecular species and dramatically lower hydrogenation selectivity. As the STM image in Fig. 2C illustrates, higher Pd coverages resulted in the formation of large Pd islands. These islands exhibited the common tendency of Pd, which has not been preconditioned with C, to decompose organic molecules and form adsorbed CH_x fragments on the surface that evolve H_2 at a higher temperature, resulting in considerably lower selectivities (*28*). The TPR measurements shown in Fig. 4C indicate that the overall conversion of styrene to ethylbenzene and surface carbon is 80% with the selectivity toward ethylbenzene being 38%. In other words, ~50% of the initially adsorbed reactant decomposed on the surface. A similar picture was observed in the case of acetylene hydrogenation on 1 ML Pd/Cu(111) (Fig. 4D); 60% of the initially dosed acetylene decomposed to form surface carbon with no coupling products observed. The overall conversion of acetylene was 90%, whereas the selectivity toward ethene was 33%.

Our results demonstrate that very small quantities of individual, isolated catalytically active metal atoms can substantially influence the catalytic properties of less reactive metals. Minority Pd atoms (1%) in a Cu surface activate hydrogen, which then populates bare Cu areas (99%) where it is weakly bound and effective for hydrogenation, yielding a bifunctional surface with different regions facilitating different steps in the reaction. From a practical application standpoint, the small amounts of precious metal required to produce SAAs generates a very attractive alternative to most traditional bimetallic catalysts. Recent advances in catalyst synthesis mean that synergistic effects, whereby different components of the catalyst have a particular function in the overall reaction mechanism, are indeed possible with practical dispersed catalysts (*29*). Implementation of the SAA approach to the design of real catalysts requires consideration of the effect of higher reaction temperature, which may cause the minority active element to segregate into the bulk of the

more inert host and hence a loss in activity. However, there are now many experimental and theoretical examples of metal alloys under realistic conditions in which the more active element is stabilized at the surface by adsorbates (*21*, *30*–*32*). This adsorbate-induced reverse segregation effect is understood in terms of the adsorbate binding more strongly to the element, which would normally segregate to the bulk and result in a reversal of the surface segregation behavior (*21*). In the case of the Cu/Pd system, the stabilization resulting from segregation of Cu to the surface is small (0.02 eV) (*31*) compared with the ~0.4-eV increase in binding of H to Pd versus Cu (*6*, *20*). The fact that Pd segregation to the Cu surface has been observed experimentally in Pd/Cu catalysts under realistic hydrogenation operating conditions bodes well for the utility of this atomic geometry in real catalysts (*32*).

References and Notes

1. S. Abbet *et al.*, *J. Am. Chem. Soc.* **122**, 3453 (2000).
2. J. C. Fierro-Gonzalez, V. A. Bhirud, B. C. Gates, *Chem. Commun.* **42**, 5275 (2005).
3. Y. Zhai *et al.*, *Science* **329**, 1633 (2010).
4. J. M. Thomas, Z. Saghi, P. L. Gai, *Top. Catal.* **54**, 588 (2011).
5. F. Besenbacher *et al.*, *Science* **279**, 1913 (1998).
6. H. L. Tierney, A. E. Baber, J. R. Kitchin, E. C. H. Sykes, *Phys. Rev. Lett.* **103**, 246102 (2009).
7. D. O. Bellisario *et al.*, *J. Phys. Chem. C* **113**, 12863 (2009).
8. H. L. Tierney, A. E. Baber, E. C. H. Sykes, *J. Phys. Chem. C* **113**, 7246 (2009).
9. Methods and additional data are available as supporting material on *Science* Online.
10. A. Bach Aaen, E. Lægsgaard, A. V. Ruban, I. Stensgaard, *Surf. Sci.* **408**, 43 (1998).
11. T. Kammler, J. Küppers, *J. Chem. Phys.* **111**, 8115 (1999).
12. I. S. Chopra, S. Chaudhuri, J. F. Veyan, Y. J. Chabal, *Nat. Mater.* **10**, 884 (2011).
13. A. Wittstock, V. Zielasek, J. Biener, C. M. Friend, M. Bäumer, *Science* **327**, 319 (2010).
14. L. J. Lauhon, W. Ho, *Phys. Rev. Lett.* **85**, 4566 (2000).
15. T. Mitsui, M. K. Rose, E. Fomin, D. F. Ogletree, M. Salmeron, *Nature* **422**, 705 (2003).
16. G. Anger, A. Winkler, K. D. Rendulic, *Surf. Sci.* **220**, 1 (1989).
17. G. E. Gdowski, T. E. Felter, R. H. Stulen, *Surf. Sci.* **181**, L147 (1987).
18. C. Sousa, V. Bertin, F. Illas, *J. Phys. Chem. B* **105**, 1817 (2001).
19. A. Roudgar, A. Groß, *Surf. Sci.* **597**, 42 (2005).
20. J. Greeley, M. Mavrikakis, *J. Phys. Chem. B* **109**, 3460 (2005).
21. J. Greeley, M. Mavrikakis, *Nat. Mater.* **3**, 810 (2004).
22. J. Knudsen *et al.*, *J. Am. Chem. Soc.* **129**, 6485 (2007).
23. O. Skoplyak, M. A. Barteau, J. G. Chen, *J. Phys. Chem. B* **110**, 1686 (2006).
24. S. Alayoglu, A. U. Nilekar, M. Mavrikakis, B. Eichhorn, *Nat. Mater.* **7**, 333 (2008).
25. J. T. Roberts, R. J. Madix, *J. Am. Chem. Soc.* **110**, 8540 (1988).
26. W. T. Tysoe, G. L. Nyberg, R. M. Lambert, *Chem. Commun.* **11**, 623 (1983).
27. G. Kyriakou, J. Kim, M. S. Tikhov, N. Macleod, R. M. Lambert, *J. Phys. Chem. B* **109**, 10952 (2005).
28. B. Brandt *et al.*, *J. Phys. Chem. C* **112**, 11408 (2008).
29. H.-L. Jiang, Q. Xu, *J. Mater. Chem.* **21**, 13705 (2011).
30. F. Tao *et al.*, *Science* **322**, 932 (2008).
31. D. Priyadarshini *et al.*, *J. Phys. Chem. C* **115**, 10155 (2011).
32. J. A. Anderson, M. Fernández-García, G. L. Haller, *J. Catal.* **164**, 477 (1996).

Acknowledgments: We thank the U.S. Department of Energy (FG02-10ER16170) for financial support, NSF (CBET 0828666) for partial support (M.B.B.) and for a Graduate Research Fellowship (A.D.J.), the Department of Education for a Graduate Assistance in Areas of National Need fellowship (E.A.L.), and Tufts University for a Tufts Collaborates Seed Grant (E.C.H.S., M.F.-S., and G.K.).

Supporting Online Material

www.sciencemag.org/cgi/content/full/335/6073/1209/DC1
Materials and Methods
SOM Text
Figs. S1 to S4
References (*33*–*37*)

27 October 2011; accepted 30 January 2012
10.1126/science.1215864

An Impactor Origin for Lunar Magnetic Anomalies

Mark A. Wieczorek,[1]* Benjamin P. Weiss,[2] Sarah T. Stewart[3]

The Moon possesses strong magnetic anomalies that are enigmatic given the weak magnetism of lunar rocks. We show that the most prominent grouping of anomalies can be explained by highly magnetic extralunar materials from the projectile that formed the largest and oldest impact crater on the Moon: the South Pole–Aitken basin. The distribution of projectile materials from a model oblique impact coincides with the distribution of magnetic anomalies surrounding this basin, and the magnetic properties of these materials can account for the intensity of the observed anomalies if they were magnetized in a core dynamo field. Distal ejecta from this event can explain the origin of isolated magnetic anomalies far from this basin.

Beginning with the Apollo era, spacecraft observations have shown that portions of the lunar crust are strongly magnetized (*1*–*4*), yet their origin has remained unresolved. The lithologies of the source rocks for these anomalies are unknown, their time of magnetization acquisition is poorly constrained, and it is unclear whether the magnetization process was thermoremanent or shock-related (*5*, *6*). As a result, the origin of the magnetizing fields is a matter of debate, with possibilities including a core dynamo, transient fields generated during impacts, and the amplification of ambient fields by impact-generated plasmas (*7*–*13*).

A key difficulty is that most lunar magnetic anomalies have not been recognized to correlate with known geologic structures. A few impact basins possess central magnetic anomalies (*12*, *14*, *15*), but these anomalies are typically weak and are not representative of the most intense anomalies, most of which are located on the far side of the Moon (Fig. 1). Impact basin ejecta deposits are statistically somewhat more magnetic than other geologic units, but the magnetic signatures of the ejecta from any given basin are quite variable (*16*). A few prominent anomalies on the far side of the Moon are located near the antipodes of four young impact basins (*2*, *3*), suggestive of an exotic impact origin (*17*), but many strong anomalies are not associated with basin antipodes, and most basins do not possess antipodal anomalies.

It is also difficult to reconcile the strengths of these anomalies with the magnetic properties of known endogenous lunar materials. This is because lunar materials are very weakly magnetic relative to terrestrial materials: The saturation remanent magnetizations of mare basalts and pristine highlands rocks are weaker than those of mid-ocean ridge basalt by two to four or more orders of magnitude (*18*, *19*). To demonstrate this, we calculated the thickness of magnetized materials required to generate a representative 10-nT anomaly at an altitude of 30 km as a function of the magnetizing field strength and rock thermoremanence susceptibility (ratio of thermoremanence to the magnetizing field) (Fig. 2). The thermoremanence susceptibility correlates with both the abundance of magnetic carriers in the rock and the rock's saturation remanent magnetization (supporting online material), and lunar paleomagnetic studies imply ancient field strengths between ~1 and 120 μT (*5*, *20*, *21*). We find that even the highest postulated paleofield strengths would require extremely thick deposits of unidirectionally magnetized materials to account for the lunar magnetic anomalies. For example, more than 100 km of pristine feldspathic highland rocks would be required, but these thicknesses are greater than the thickness of the entire lunar crust. More than 10 km of mare basalts would be required, but this far exceeds the thickness of most maria (*11*). Even the relatively highly magnetic mafic impact melts, most of which are thought to be derived from the Imbrium impact event (*22*), would require thicknesses of at least several kilometers, but none of the magnetic anomalies show the topographic expressions that might be expected for such locally thick ejecta deposits.

However, there is a major geologic structure that correlates with some of the largest lunar magnetic anomalies and that has received little consideration previously. The far-side hemisphere of the Moon hosts the largest known unequivocal

[1]Institut de Physique du Globe de Paris, Université Paris Diderot, 94100 Saint-Maur des Fossés, France. [2]Department of Earth, Atmospheric, and Planetary Sciences, Massachusetts Institute of Technology, Cambridge, MA 02139, USA. [3]Department of Earth and Planetary Sciences, Harvard University, Cambridge, MA 02138, USA.

*To whom correspondence should be addressed. E-mail: wieczor@ipgp.fr